Supporting Information

Lithium hydride synergy with Fe/N-co-doped porous carbon for efficient ammonia synthesis

Yefei Wang, Fei Chang*

Yongjiang Laboratory, Ningbo 315202, China

*Corresponding author E-mail address: fei-chang@ylab.ac.cn

This file includes:

Fig. S1-S23

Tables S1-S4

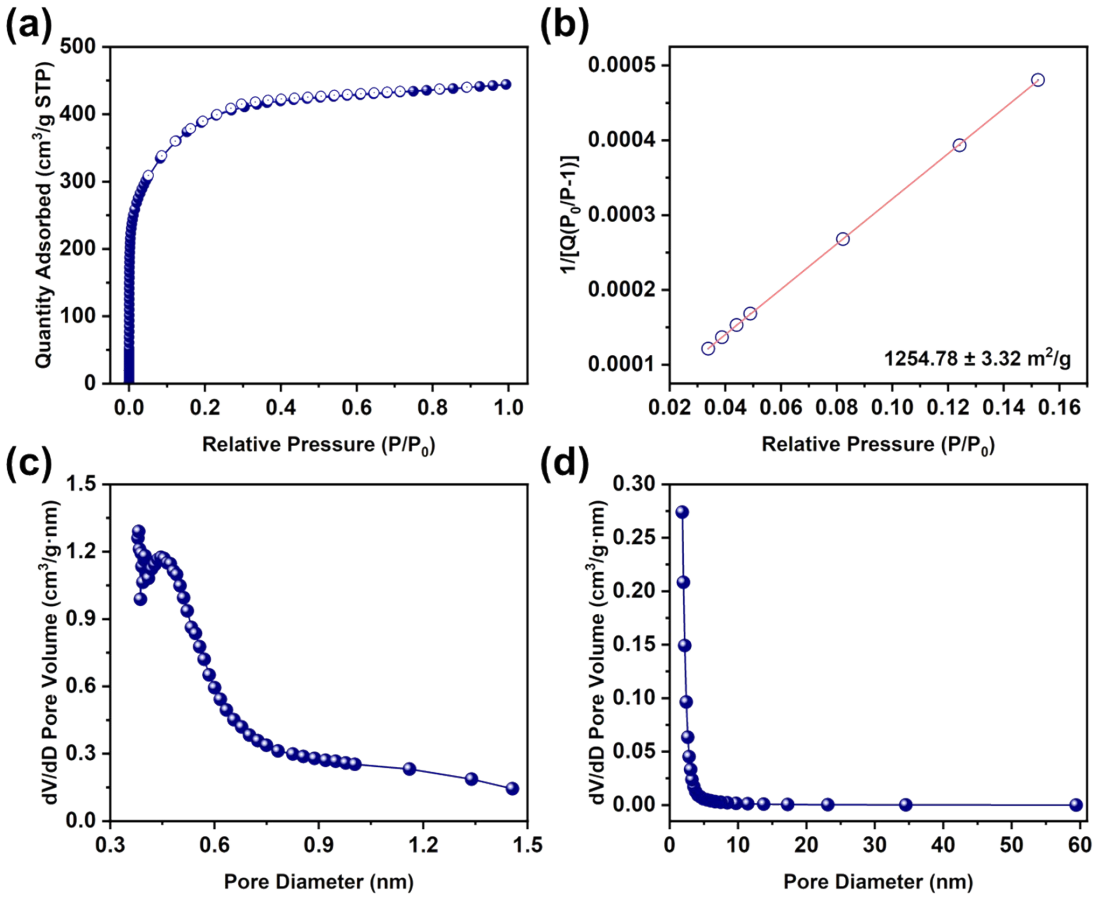

Fig. S1 (a) Argon isotherm linear plot for Fe-N-C at 77 K. (b) Plot of the linear region on the argon isotherm of Fe-N-C for the BET equation. (c,d) Pore size distribution of Fe-N-C using data measured with argon at 77 K.

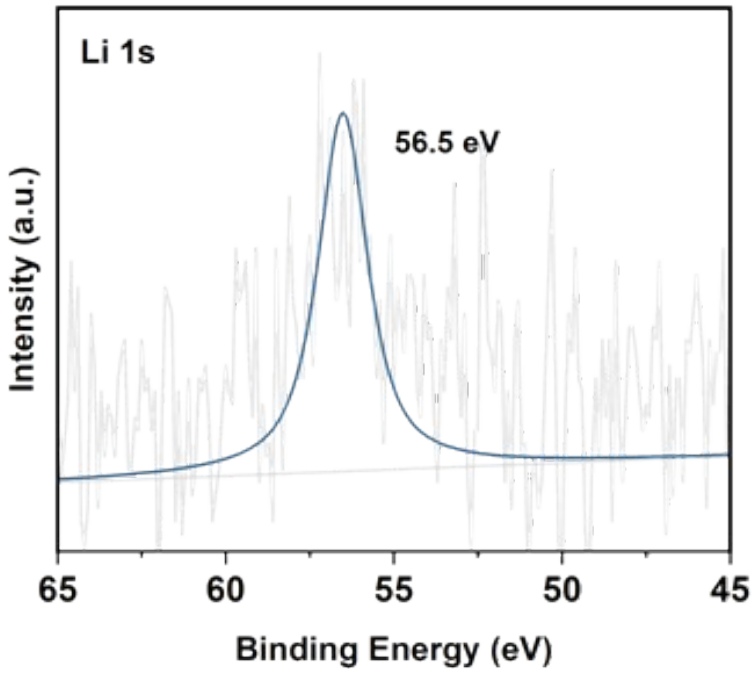

Fig. S2 The Li 1s XPS spectrum of LiH/Fe-N-C.

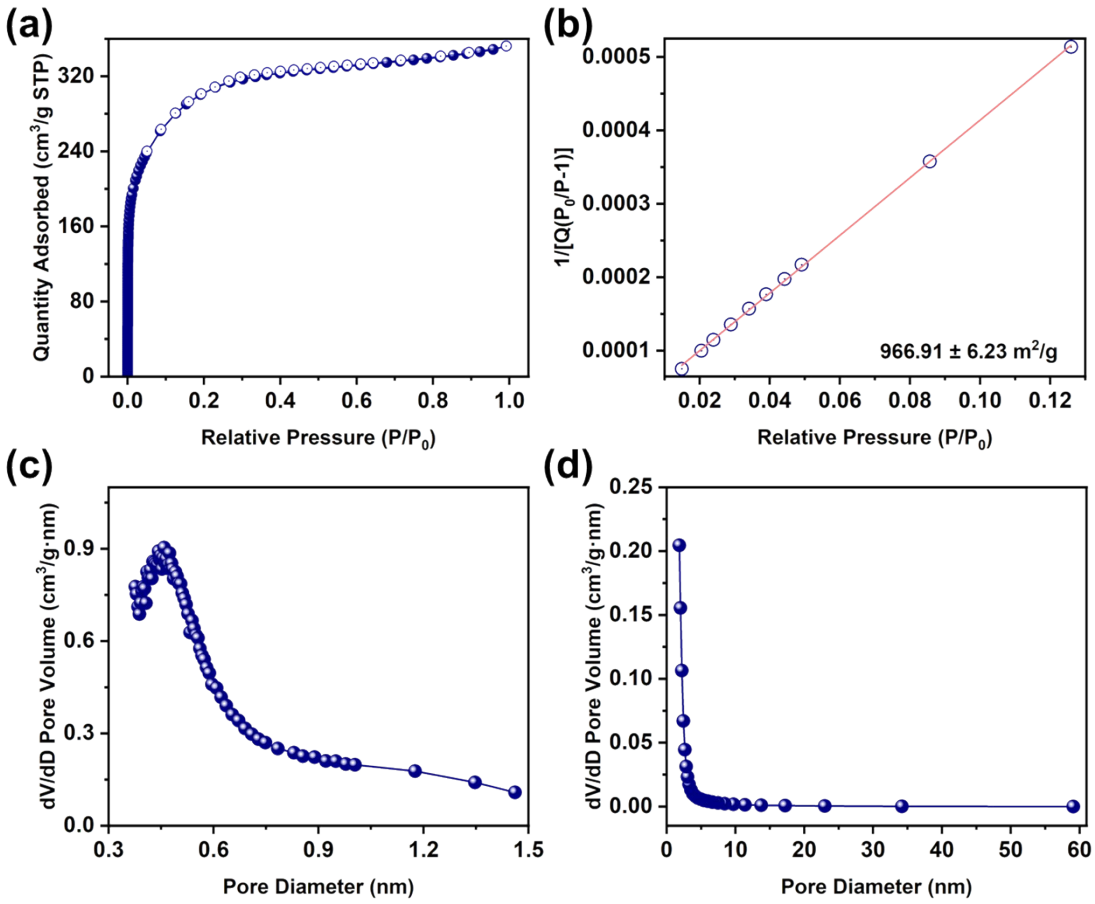

Fig. S3 (a) Argon isotherm linear plot for LiH/Fe-N-C at 77 K. (b) Plot of the linear region on the argon isotherm of LiH/Fe-N-C for the BET equation. (c,d) Pore size distribution of LiH/Fe-N-C using data measured with argon at 77 K.

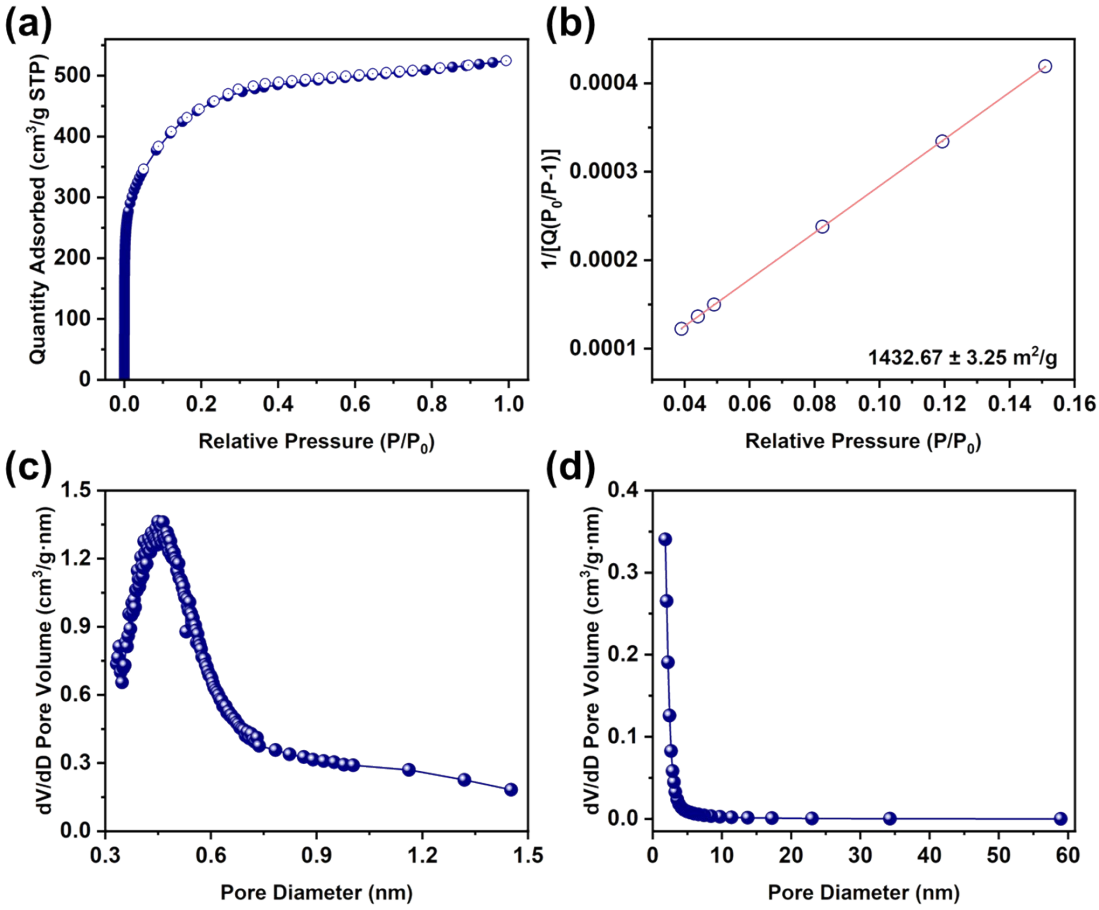

Fig. S4 (a) Argon isotherm linear plot for N-C at 77 K. (b) Plot of the linear region on the argon isotherm of N-C for the BET equation. (c,d) Pore size distribution of N-C using data measured with argon at 77 K.

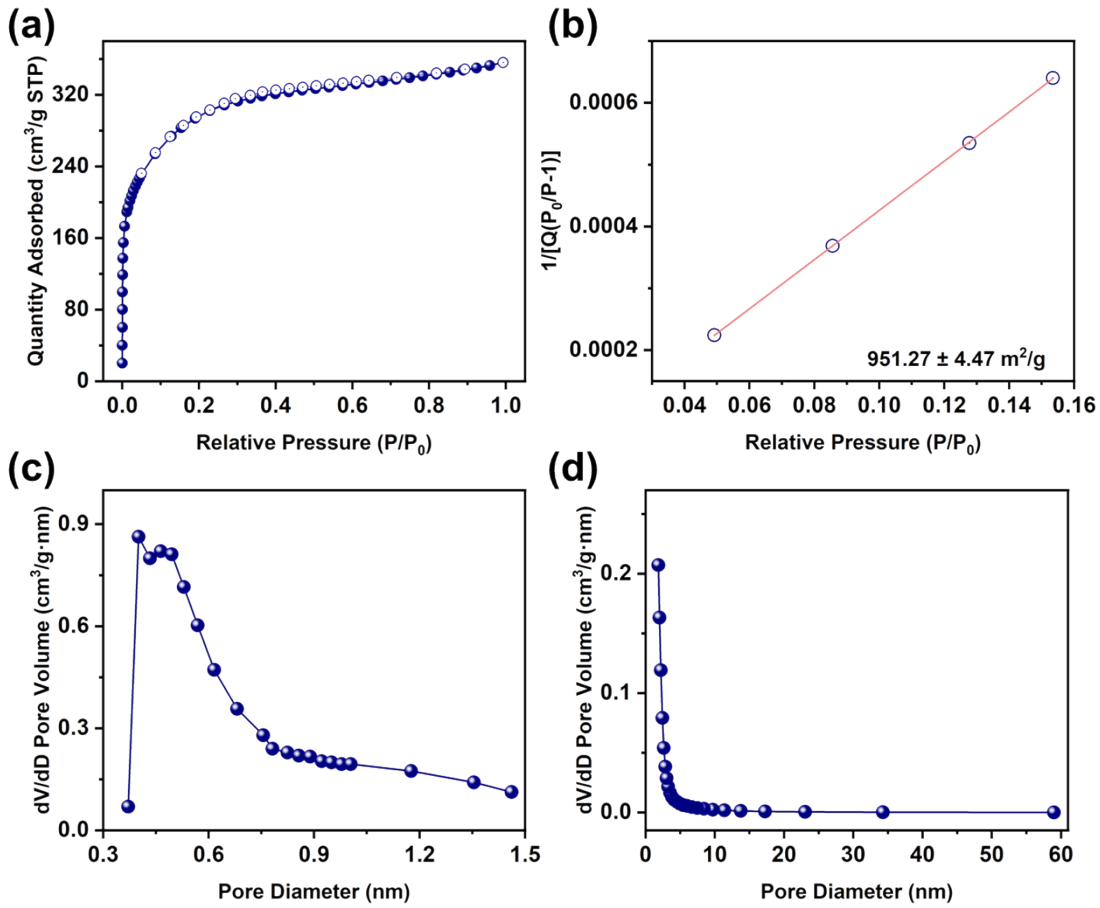

Fig. S5 (a) Argon isotherm linear plot for LiH/N-C at 77 K. (b) Plot of the linear region on the argon isotherm of LiH/N-C for the BET equation. (c,d) Pore size distribution of LiH/N-C using data measured with argon at 77 K.

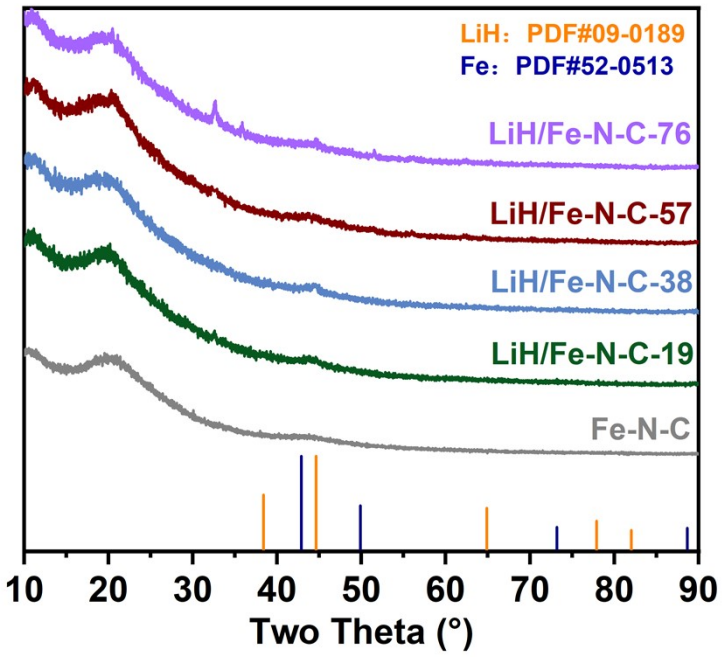

Fig. S6 XRD patterns of Fe-N-C, and LiH/Fe-N-C-X (X represents the molar ratio of Li/Fe).

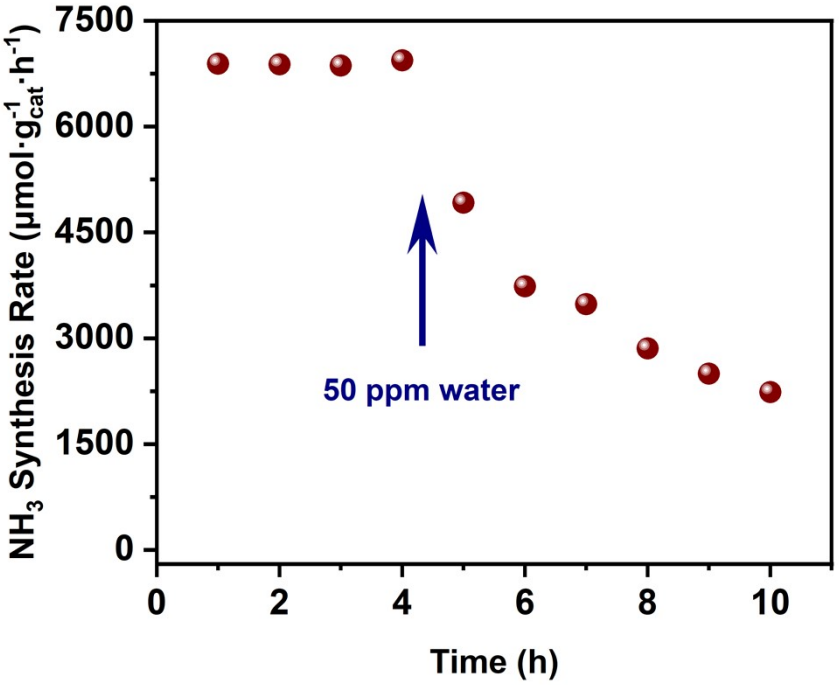

Fig. S7. Stability test of the LiH/Fe-N-C at 300 °C under 1.0 MPa with the presence of 50 ppm water in the feed gas.

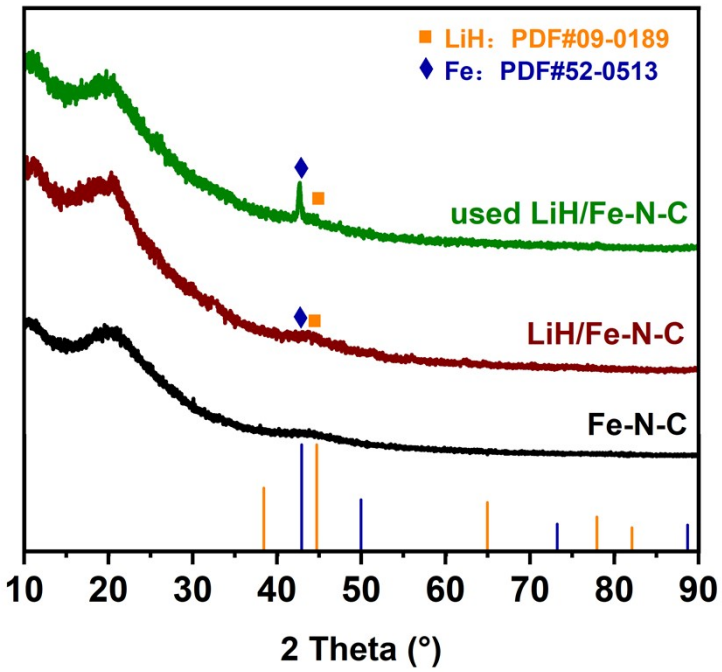

Fig. S8 XRD patterns for Fe-N-C, LiH/Fe-N-C and LiH/Fe-N-C after ammonia synthesis reaction (reaction conditions: catalyst (50 mg), synthesis gas (H_2/N_2 = 3, 50 $mL \cdot min^{-1}$), temperature (300 °C), pressure (1.0 MPa), time (50 h)).

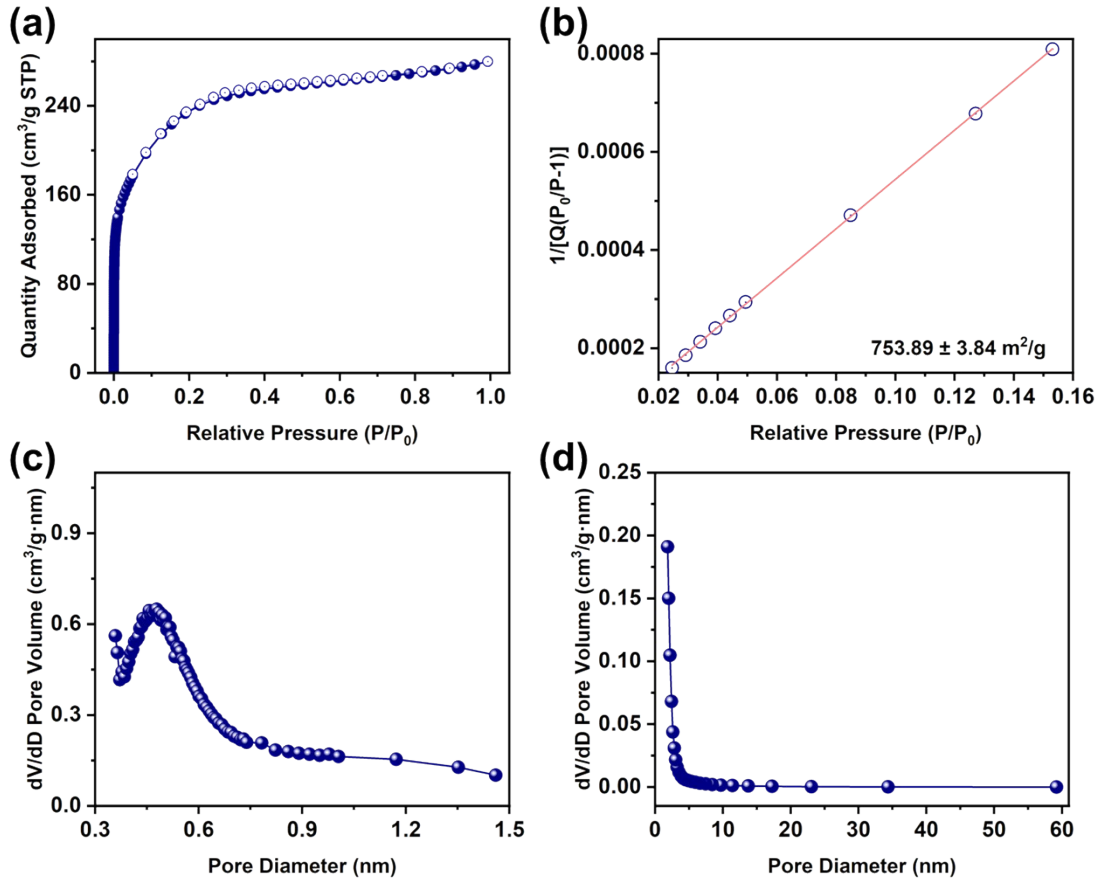

Fig. S9 (a) Argon isotherm linear plot for used LiH/Fe-N-C at 77 K. (b) Plot of the linear region on the argon isotherm of used LiH/Fe-N-C for the BET equation. (c,d) Pore size distribution of used LiH/Fe-N-C using data measured with argon at 77 K.

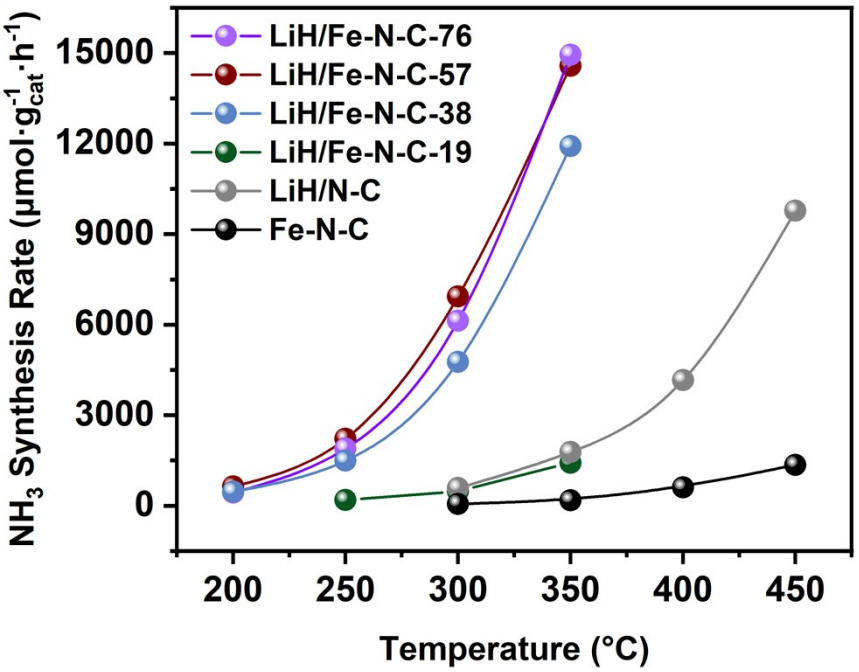

Fig. S10 NH_3 synthesis rates of LiH/Fe-N-C-X, Fe-N-C, and LiH/N-C as a function of temperatures. Reaction conditions: N_2:H_2 = 1:3 with a WHSV of 60,000 ml g^{-1} h^{-1}; pressure,1 MPa.

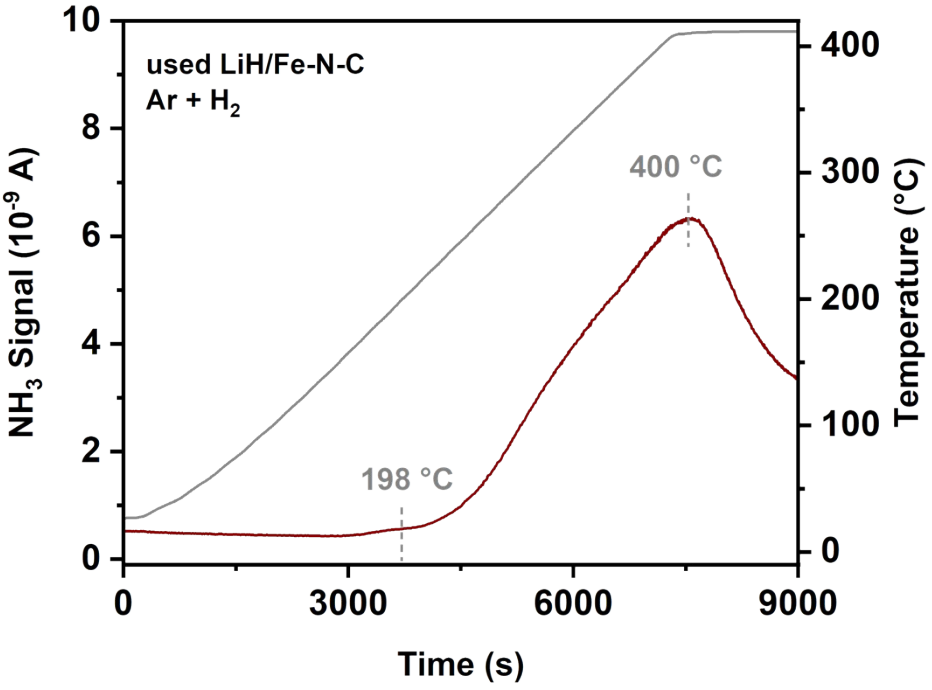

Fig. S11 H_2-TPR profile of used LiH/Fe-N-C.

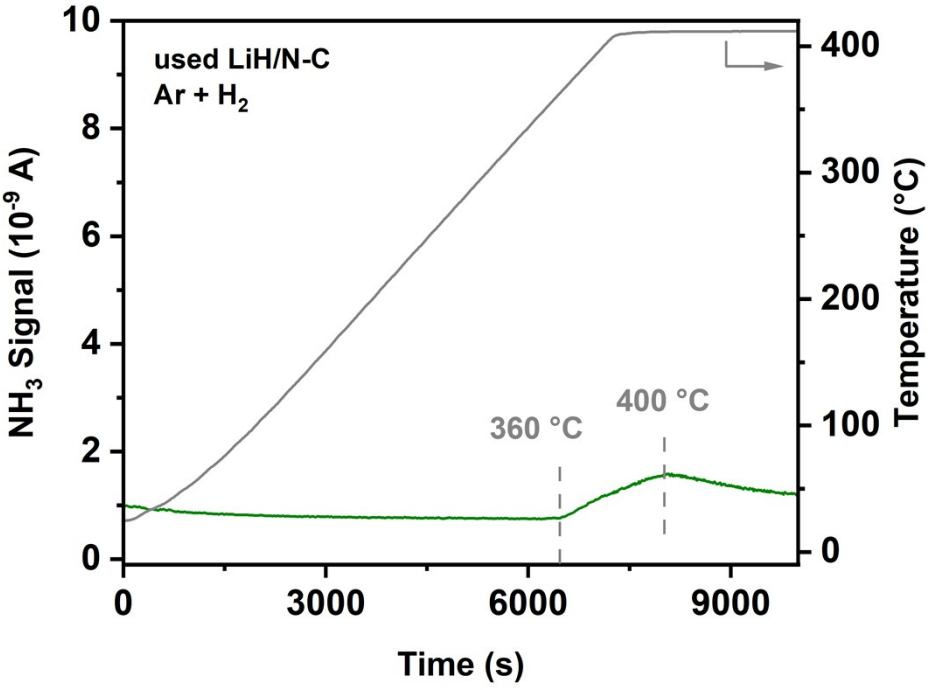

Fig. S12 H_2-TPR profile of used LiH/N-C.

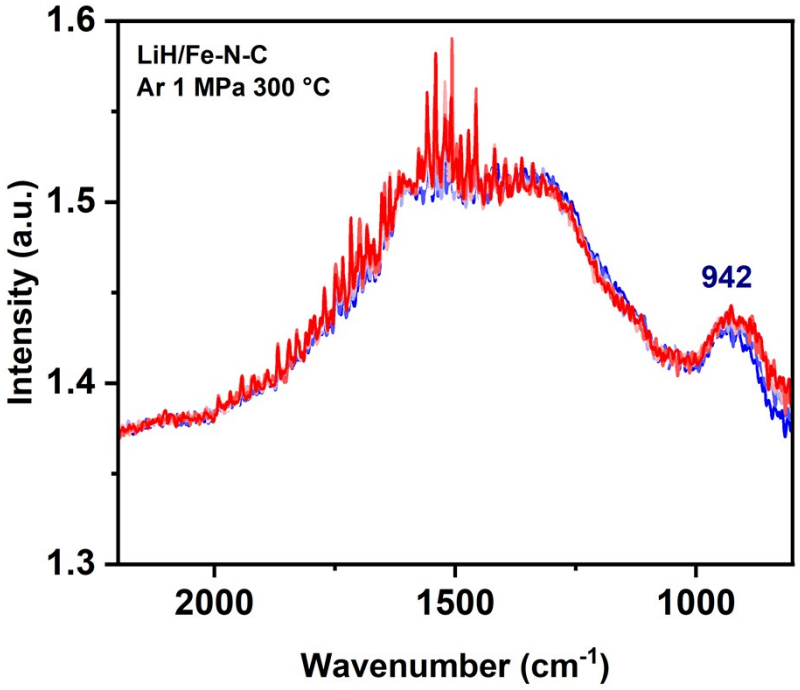

Fig. S13 In situ DRIFTS of LiH/Fe-N-C at 300 °C under 1 MPa in the stream of argon.

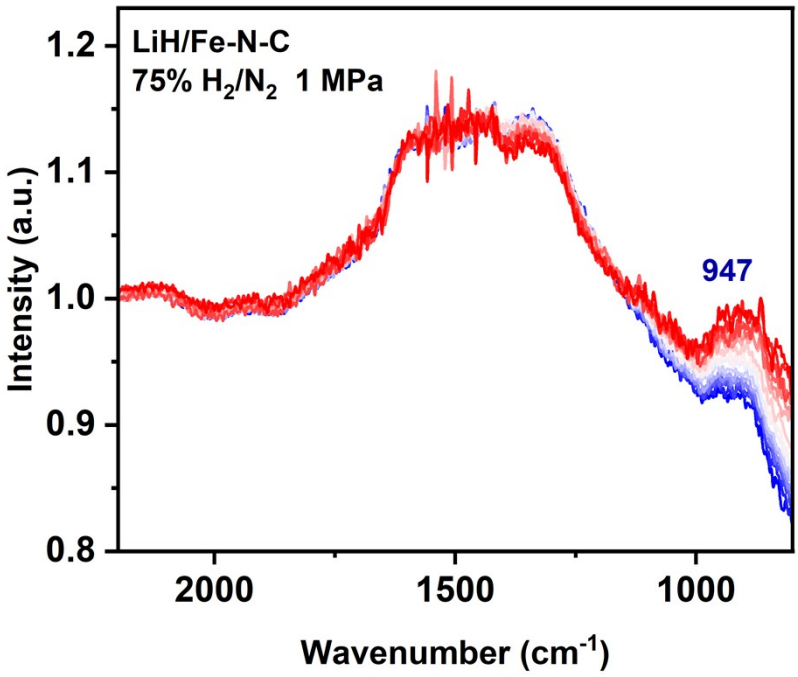

Fig. S14 In situ DRIFTS of LiH/Fe-N-C in the reaction condition (75% H_2/N_2 stream, 1.0 MPa, from 25 °C (blue line) to 300 °C (red line)).

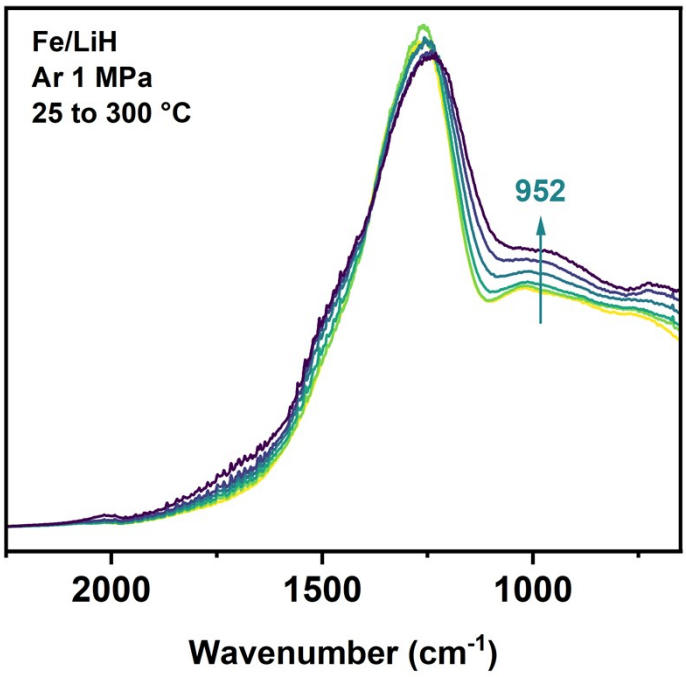

Fig. S15 In situ DRIFTS of Fe/LiH bulk composite at the temperature from 25 to 300 °C under 1 MPa in the stream of argon.

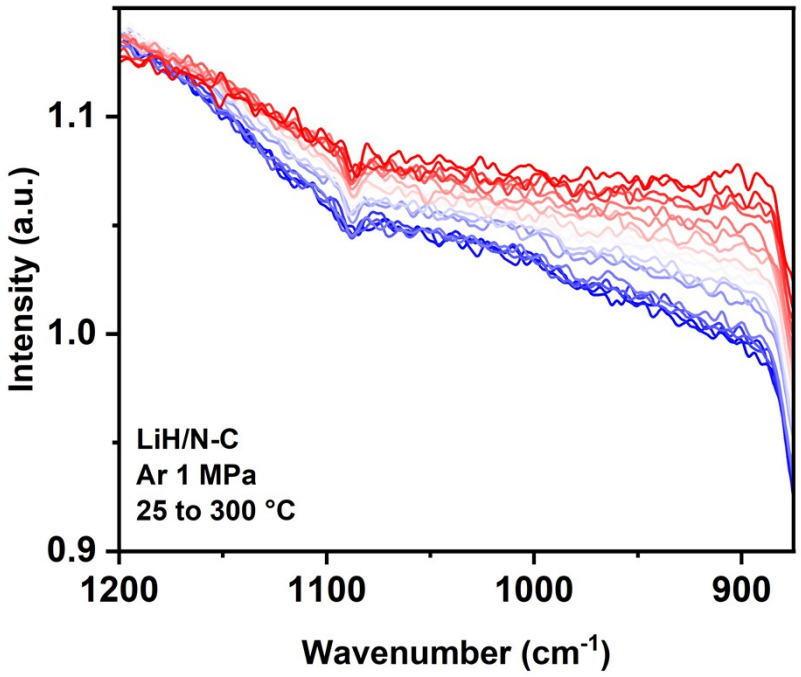

Fig. S16 In situ DRIFTS of LiH/N-C at the temperature from 25 to 300 °C under 1 MPa in the stream of argon.

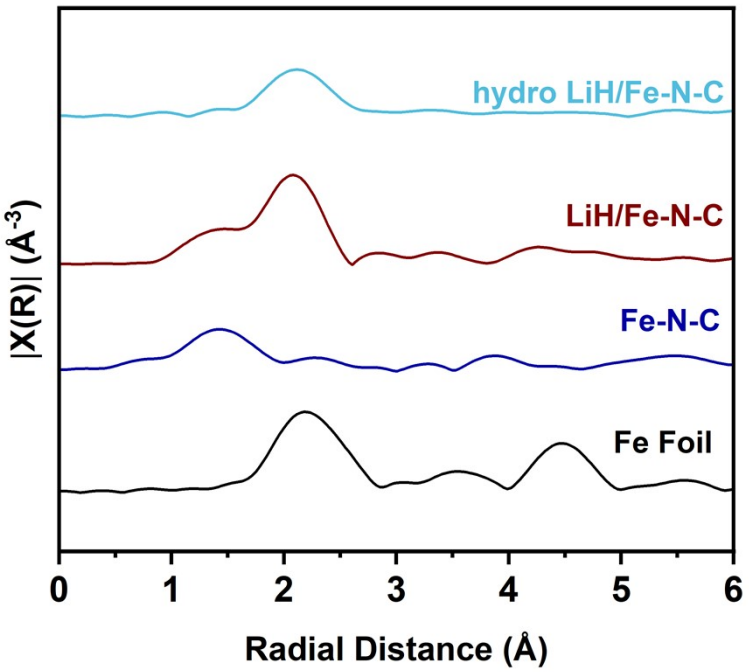

Fig. S17 EXAFS spectrum of hydro LiH/Fe-N-C. LiH/Fe-N-C and Fe-N-C was included as reference.

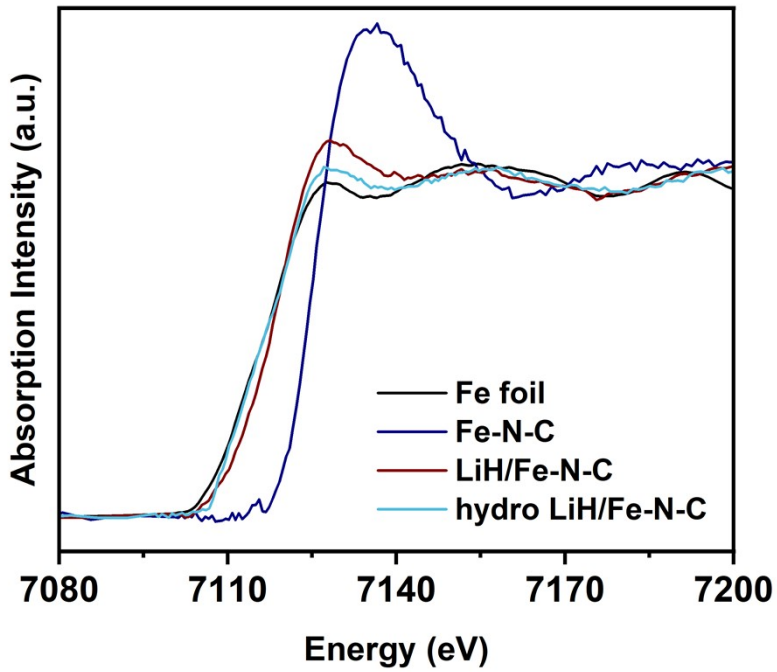

Fig. S18 Fe K-edge XANES profiles of the hydro LiH/Fe-N-C sample. LiH/Fe-N-C and Fe-N-C was included as reference.

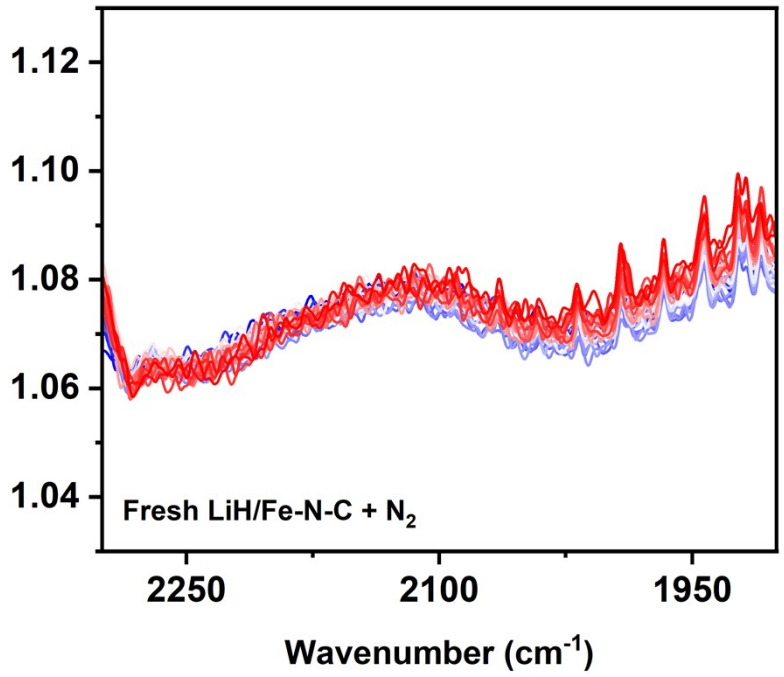

Fig. S19 in situ DRIFTS of fresh LiH/Fe-N-C in N_2 stream under 1.0 MPa at the temperature from 25 °C (blue) to 300 °C (red).

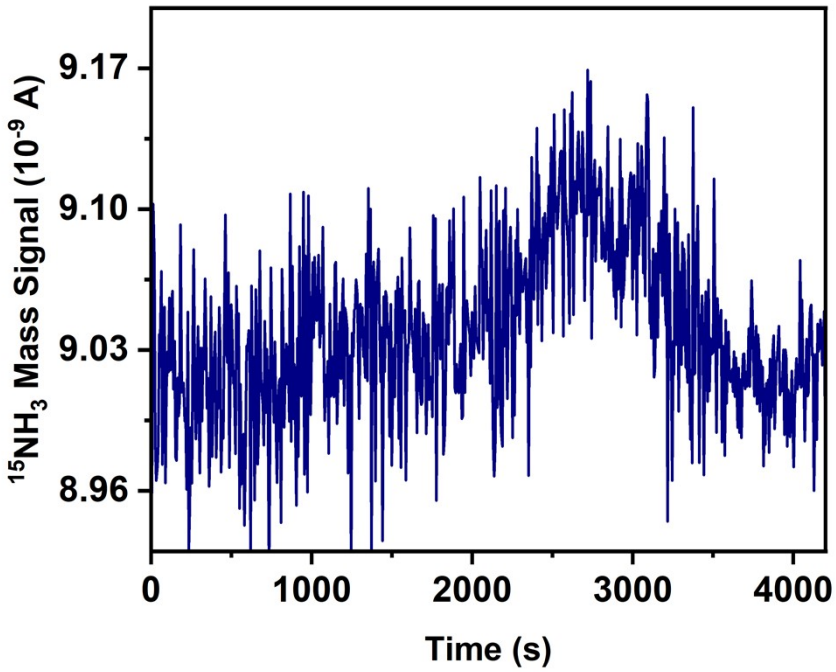

Fig. S20. H_2-temperature programmed reduction (H_2-TPR) profiles of LiH/Fe-N-C after hydrogenation in a flow of H_2/Ar (3:1) at 1 MPa and 300 °C, followed by pre-treatment in 0.2 MPa $^{15}N_2$.

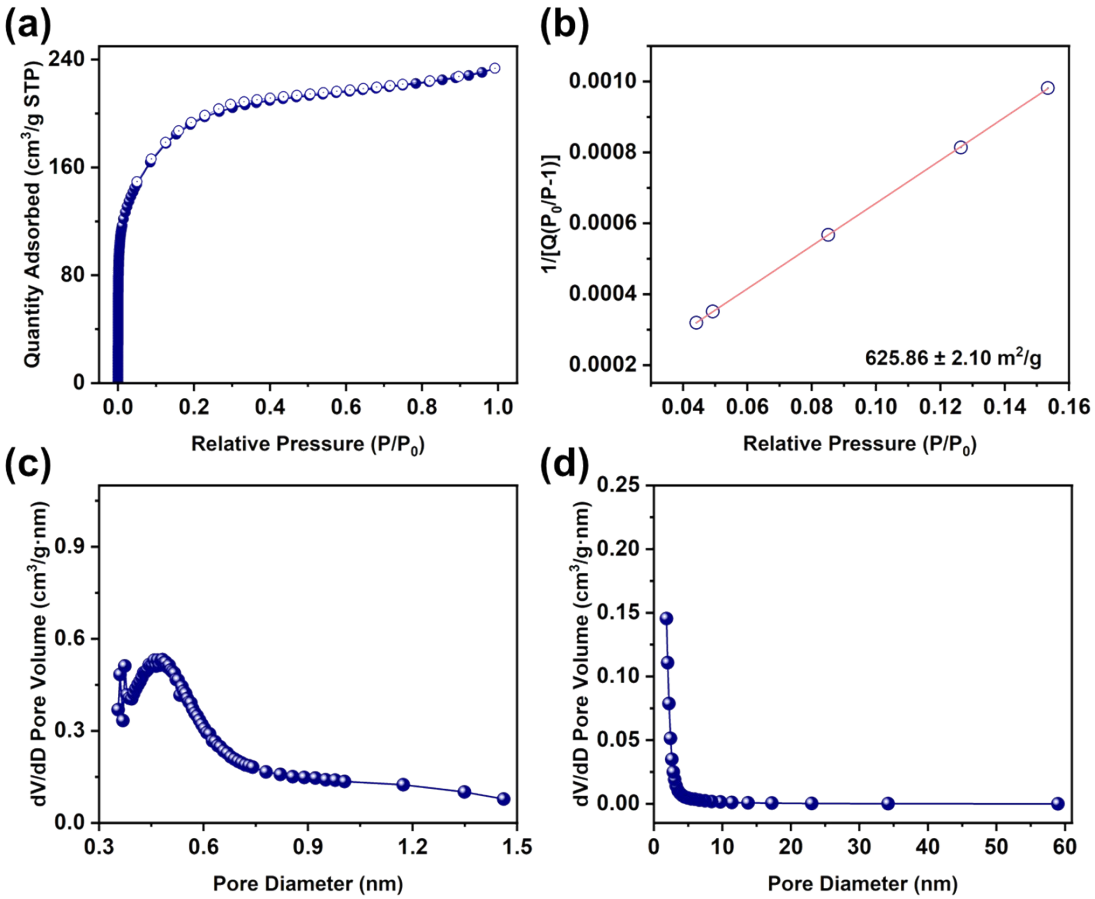

Fig. S21 (a) Argon isotherm linear plot for hydro LiH/Fe-N-C at 77 K. (b) Plot of the linear region on the argon isotherm of hydro LiH/Fe-N-C for the BET equation. (c,d) Pore size distribution of hydro LiH/Fe-N-C using data measured with argon at 77 K.

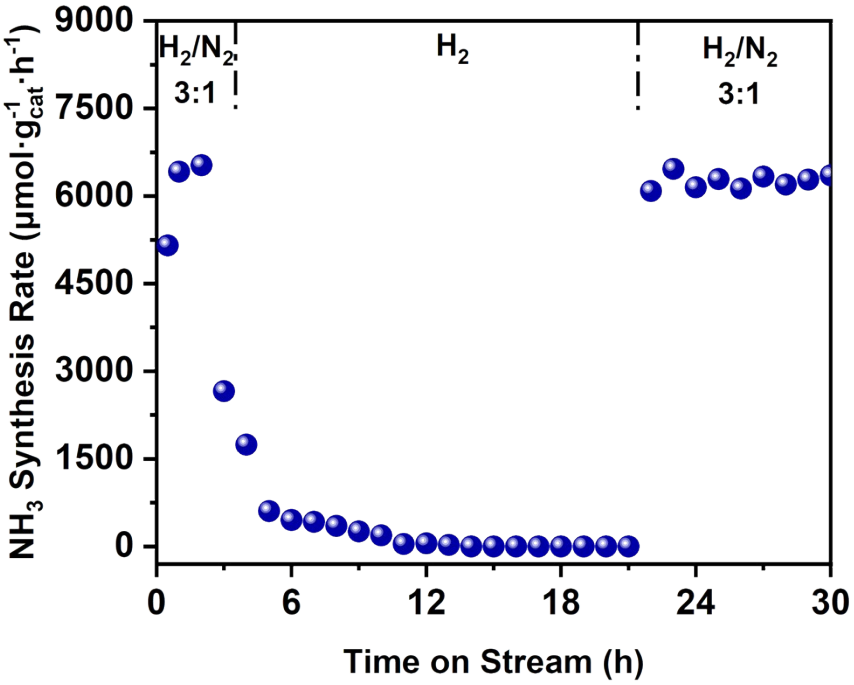

Fig. S22 Catalytic behavior of LiH/Fe-N-C at 300 °C under 1.0 MPa in the stream of 75% H_2/N_2 or pure H_2. Reaction conditions: reactant gas, 75% H_2/N_2 and pure H_2; pressure, 1.0 MPa; space velocity, 60000 mL g_{cat}^{-1} h^{-1}.

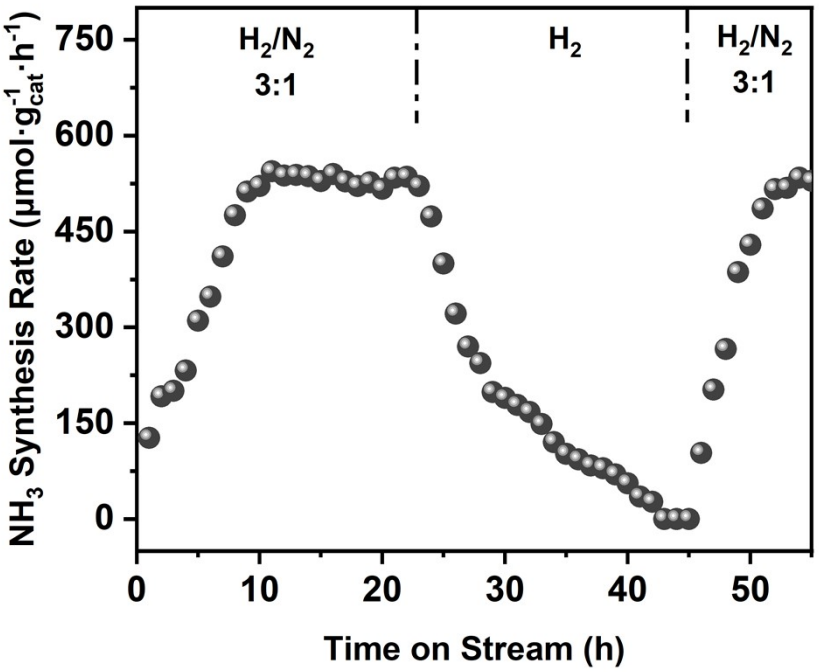

Fig. S23 Catalytic behavior of LiH/N-C at 300 °C under 1.0 MPa in the stream of 75% H_2/N_2 or pure H_2. Reaction conditions: reactant gas, 75% H_2/N_2 and pure H_2; pressure, 1.0 MPa; space velocity, 60000 mL g_{cat}^{-1} h^{-1}.

Table S1. ICP results of Fe-N-C, LiH/Fe-N-C, and LiH/N-C.

Sample	Fe (wt%)	Zn (wt%)	Li (wt%)
Fe-N-C	1.0024	5.0276	-
LiH/Fe-N-C	0.7768	3.8719	5.5659
LiH/N-C	-	4.2763	6.2723

Table S2. Summary of surface area, pore volume, and pore width of Fe-N-C, LiH/Fe-N-C, used LiH/Fe-N-C, hydro LiH/Fe-N-C, N-C, and LiH/N-C.

Sample	BET Surface Area ($m^2 \cdot g^{-1}$)	Micropore Volume ($cm^3 \cdot g^{-1}$)	Mesoporous Volume ($cm^3 \cdot g^{-1}$)	Median Pore Width (nm)
Fe-N-C	1254.7836	0.544441	0.215857	0.5697
LiH/Fe-N-C	966.9102	0.415565	0.171929	0.5742
hydro LiH/Fe-N-C	625.8647	0.268896	0.130798	0.6022
used LiH/Fe-N-C	753.8897	0.328470	0.158310	0.6039
N-C	1432.6718	0.610924	0.298066	0.5778
LiH/N-C	951.2733	0.420478	0.193289	0.5800

Table S3. EXAFS data fitting results of Fe foil, Fe-N-C, LiH/Fe-N-C, hydro LiH/Fe-N-C, and used Fe-N-C/Li samples.

Sample	Shell	CN	R (Å)	$\sigma^2 \times 10^2$ (Å^2)	ΔE_0 (eV)	R factor
Fe foil	Fe-Fe	8	2.46±0.01	0.34±0.25	2.90±3.33	0.011
		6	2.86±0.01	0.24±0.41		
Fe-N-C	Fe-N	4.24±1.63	1.94±0.12	0.32±0.49	-0.32±5.61	0.039
LiH/Fe-N-C	Fe-Fe	7.17±1.38	2.48±0.02	0.71±0.18	-7.88±2.56	0.018
	Fe-N	3.53±2.26	1.88±0.07	0.25±0.69		
hydro LiH/Fe-N-C	Fe-Fe	6.78±0.79	2.52±0.04	1.41±0.15	3.97±1.11	0.021
used LiH/Fe-N-C	Fe-Fe	6.97±2.07	2.55±0.08	1.20±0.34	-3.23±3.52	0.052
	Fe-N	3.84±2.27	1.82±0.07	0.55±0.79		

Table S4. A summary and comparison of advanced iron-related thermal ammonia synthesis systems.

Catalysts	Reaction Condition	Space Velocity ($mL \cdot g^{-1} \cdot h^{-1}$)	Fe Loading (wt%)	NH_3 Synthesis Rate ($\mu mol \cdot g_{cat}^{-1} \cdot h^{-1}$)	NH_3 Synthesis Rate ($mmol \cdot g_{Fe}^{-1} \cdot h^{-1}$)	Ref.
LiH/Fe-N-C	**350 °C, 1.0 MPa**	**60000**	**0.78**	**14580**	**1869**	**This work**
	300 °C, 1.0 MPa	**72000**		**7200**	**923**	
		60000		**6800**	**872**	
		30000		**4600**	**590**	
		12000		**2850**	**365**	
	300 °C, 0.1 MPa	**60000**		**1260**	**162**	
FeN_4©G-K	190 °C, 0.1 MPa	30000	2.1	10.3	0.49	[1]
Fe_{HL}-N-C	300 °C, 0.1 MPa	30000	2.39	558	23	[2]
Fe-$BaCeO_{3-x}N_yH_z$	300 °C, 0.9 MPa	36000	1.2	1800	150	[3]
6K-$FePc_{80}CoPc_{20}$	300 °C, 1.0 MPa	12000	30	3000	10	[4]
AlH-K^+/Fe	300 °C, 1.0 MPa	36000	~97	8500	8.8	[5]
BaH_2-BaO/Fe/CaH_2	300 °C, 1.0 MPa	36000	~10	5500	55	[6]
Fe-5LiH/MgO	300 °C, 1.0 MPa	60000	~5.8	~7000	120	[7]
Fe/K(3)/MgO-500red	300 °C, 1.0 MPa	72000	15.3	9200	60	[8]
Fe/Ba(1)/MgO-700red	300 °C, 1.0 MPa	72000	16.2	7100	44	[9]
FeOOH−K/Al_2O_3	325 °C, 9.0 MPa	12000	21.8	1880	8.6	[10]
10-$CsFePc_{600}$	400 °C, 1.0 MPa	12000	30	7800	26	[11]
Co/Fe-CeO_2	400 °C, 1.0 MPa	60000	1.7	3620	212	[12]
Fe/$BaTiO_{2.35}H_{0.65}$	400 °C, 1.0 MPa	60000	0.40	5700	1425	[13]

References

1. Z. Chen, Y. Ye, T. Peng, C. Wu, H. Li, X. Pan and X. Bao, *ACS Catal.*, 2023, **13**, 14385-14394.
2. Y. Jiang, Z. Chen, T. Peng, L. Jiao, X. Pan, X. Bao and H.-L. Jiang, *Angew. Chem. Int. Ed.*, 2025, **64**, e202501190.
3. M. Kitano, J. Kujirai, K. Ogasawara, S. Matsuishi, T. Tada, H. Abe, Y. Niwa and H. Hosono, *J. Am. Chem. Soc.*, 2019, **141**, 20344-20353.
4. R. K. Rai, W. Al Maksoud, N. Morlanés, M. Harb, R. Ahmad, A. Genovese, M. N. Hedhili, L. Cavallo and J.-M. Basset, *ACS Catal.*, 2022, **12**, 587-599.
5. M. Hattori, K. Miyashita, Y. Nagasawa, R. Suzuki and M. Hara, *Adv. Sci.*, 2025, **12**, 2410313.
6. M. Hattori, N. Okuyama, H. Kurosawa and M. Hara, *J. Am. Chem. Soc.*, 2023, **145**, 7888-7897.
7. P. Wang, H. Xie, J. Guo, Z. Zhao, X. Kong, W. Gao, F. Chang, T. He, G. Wu, M. Chen, L. Jiang and P. Chen, *Angew. Chem. Int. Ed.*, 2017, **56**, 8716-8720.
8. K. Era, K. Sato, S. i. Miyahara, T. Naito, K. De Silva, S. Akrami, H. Yamada, T. Toriyama, T. Yamamoto, Y. Murakami, K. i. Aika, K. Inazu and K. Nagaoka, *ChemSusChem*, 2023, **16**, e202300942.
9. K. Era, K. Sato, S.-i. Miyahara, T. Naito, K. De Silva, S. Akrami, H. Yamada, T. Toriyama, T. Tamaoka, T. Yamamoto, Y. Murakami, K. Inazu and K. Nagaoka, *Sustainable Energy Fuels*, 2024, **8**, 2593-2600.
10. H. Fan, X. Huang, K. Kähler, J. Folke, F. Girgsdies, D. Teschner, Y. Ding, K. Hermann, R. Schlögl and E. Frei, *ACS Sustainable Chem. Eng.*, 2017, **5**, 10900-10909.
11. W. Al Maksoud, R. K. Rai, N. Morlanés, M. Harb, R. Ahmad, S. Ould-Chikh, D. Anjum, M. N. Hedhili, B. E. Al-Sabban, K. Albahily, L. Cavallo and J.-M. Basset, *J. Catal.*, 2021, **394**, 353-365.
12. G. Zhong, Y. Liu, S. Yu, C. Zhang, J. Ni, J. Lin, B. Lin and L. Jiang, *Ind. Eng. Chem. Res.*, 2024, **63**, 5089-5096.
13. Y. Tang, Y. Kobayashi, N. Masuda, Y. Uchida, H. Okamoto, T. Kageyama, S. Hosokawa, F. Loyer, K. Mitsuhara, K. Yamanaka, Y. Tamenori, C. Tassel, T. Yamamoto, T. Tanaka and H. Kageyama, *Adv. Energy Mater.*, 2018, **8**, 1801772.